Tuijin Jishu/Journal of Propulsion Technology
ISSN: 1001-4055
Vol. 47 No. 01 (2026)

Development of a Novel Analytical Framework for Investigating Non-symmetric Deformation Behavior in Strip Rolling

P Gopalakrishnaiah[1*], Ch. Srinivasarao[2], Anupama Francy Kothasiri[3]

[1*] *Research scholar, Department of Mechanical Engineering, Andhra university, Andhra Pradesh, India*

[2] *Professor, Department of Mechanical Engineering, Andhra University, Andhra Pradesh, India*

[3] *Associate professor, Vishnu Institute of Technology, Bhimavaram, Andhra Pradesh, India*

Abstract:- In recent years, the asymmetrical rolling process has attracted considerable research attention due to its ability to induce non-uniform deformation characteristics within metallic workpieces. In this context, the present study introduces a novel analytical framework for asymmetrical cold rolling based on an enhanced slab method, specifically designed to overcome the inherent limitations of existing analytical models when applied to a wide range of asymmetric rolling conditions. A newly developed mathematical formulation for the asymmetric slab rolling process is proposed, offering a more comprehensive representation of the deformation mechanics. Unlike conventional approaches, the modified model identifies the emergence of three distinct deformation regions within the roll bite: the backward slip zone (BSZ), the forward slip zone (FSZ), and a newly characterized cross-shear zone (CSZ). This zonal classification provides deeper insight into the complex material flow behavior unique to asymmetric rolling. The study systematically investigates the influence of critical rolling parameters—including thickness reduction, roll speed ratio, applied tensions, and friction coefficient—on the configuration and evolution of these deformation zones. It is demonstrated that at specific critical roll speed ratios and tension levels, distinct deformation zone configurations are established, validating the adaptability of the proposed model under varying process conditions. Furthermore, the interdependence between deformation zone configurations and rolling parameters is elucidated through comprehensive process maps, which illustrate the variation of critical speed ratios and critical tensions across diverse rolling scenarios. To quantify the relative influence of process variables, Grey Relational Analysis (GRA) is employed, revealing that the roll velocity ratio is the most dominant factor governing rolling responses, contributing 80% to overall performance optimization. The front tension emerges as the second most influential parameter, accounting for 8.64%, and plays a supportive role in enhancing process stability and surface integrity. The analytical predictions of the proposed model are rigorously validated through confirmation experiments, demonstrating strong agreement with theoretical outcomes. Based on the GRA-derived optimal parameter set, the study recommends specific operating conditions that effectively minimize roller surface damage while simultaneously improving the surface quality of the rolled product.

Keywords*: Asymmetric strip rolling, Slab method, Energy transfer, Friction-stress, Optimization, Neutral point.*

1. Introduction

Analytical, numerical, and experimental studies must be thoroughly reviewed in order to gain a systematic understanding of metal rolling, deformation behavior, and the resulting microstructure–property relationships. The fundamental framework for forecasting deformation mechanics, roll force, torque, and frictional behavior in both symmetric and asymmetric rolling was established by the development of theoretical modeling techniques, specifically the Upper Bound Method (UBM) and the Slab Method. Concurrent advancements in thermo-mechanical processing, such as cold, cryogenic, and non-isothermal rolling, have improved our knowledge of temperature-dependent flow characteristics, strain accumulation, and grain refinement in high-strength aluminum alloys like AA7075. The relationships between precipitation, recovery, and recrystallization phenomena under

different heat-treatment conditions, such as homogenization, solutionizing, and artificial aging, are highlighted by research on microstructural evolution. The significant impact of alloying additions (Zn, Mg, Cu, Sc), thermal history, and mechanical processing routes on environmental degradation behavior, fracture limits, and tribological performance is also demonstrated by studies on corrosion, formability, and wear of 7xxx series alloys. Together, these contributions provide the scientific foundation for understanding the reactions of heat-treated AA7075 and AA7075-Sc alloys as well as for modeling and improving rolling processes. The following subsections summarize this information in accordance with the major thematic areas that are pertinent to the current study.

1.1 Mathematical Modelling in Rolling

Understanding the deformation mechanics, force requirements, and process responses associated with metal rolling operations is largely dependent on mathematical modeling. Analytical and numerical models offer a crucial framework for forecasting the behavior of the strip and the load conditions acting on the rolls because rolling is controlled by intricate interactions between material flow, contact friction, strain hardening, and thermal effects

1.1.1 Upper Bound Method (UBM)

In metal rolling, the Upper Bound Method has been crucial in forecasting strain fields, power consumption, and deformation mechanics. The minimum power needed for cold strip rolling was first measured using UBM by Avitzur et al. (1963), who showed that velocity field assumptions have a significant impact on predicted friction and deformation energy [1]. This method was later improved by Avitzur (1964), who demonstrated that the admissible velocity field can be divided into distinct deformation zones, each of which represents a kinematically acceptable strain pattern during rolling [2]. The technique was expanded by Lin and Lin (1995) to forecast rolling force and strip shape changes in three dimensions, highlighting the impact of friction asymmetry and thermal softening on deformation fields [3]. In order to demonstrate how deformation energy estimates could assist real-time control strategies, Baxter and Bumby (1995) applied UBM principles to systems engineering models of strip rolling control [4]. Al-Salehi et al. (1973) verified that UBM-based estimates correctly predicted the location of neutral points in cold rolling by experimentally establishing roll pressure distributions [5].

A comprehensive power-analysis framework suitable for both symmetrical and asymmetrical rolling conditions was presented by Avitzur (1996), who combined previous formulations [6]. Later, Avitzur and Pachla (1986) showed that it was possible to increase prediction accuracy in plane-strain rolling by superimposing both rotational and linear velocity fields [7]. By suggesting a continuous velocity field devoid of discontinuities, Lambert et al. (1969) made a substantial advancement that allowed for more accurate predictions of steady-state plastic flow [8]. By highlighting how deformation energy controls industrial rolling throughput, Barbosa-Filho (2000) demonstrated how demand-driven models could be combined with UBM frameworks for macro-scale productivity simulations [9]. UBM and finite-element concepts were successfully combined by Hsiang and Lin (2000), showing that hybrid analytical–numerical approaches could improve shape rolling prediction accuracy [10]. In order to enhance predictive capability under contemporary rolling conditions involving high reductions, frictional asymmetry, and temperature-dependent material behavior, recent studies have reexamined the Upper Bound Method. When compared to traditional formulations, Montmitonnet (2016) noted that improved admissible velocity fields greatly increase the accuracy of power and torque predictions in strip rolling [11]. Incorporating strain-rate-sensitive flow stress into UBM formulations improves prediction reliability for aluminum alloy rolling under non-isothermal conditions, as Wang et al. (2018) showed [12]. According to Dixit and Mishra (2020), UBM-based analytical models successfully capture the impact of roll geometry and friction factor on the maximum reduction that can be achieved when cold rolling high-strength aluminum alloys [13]. Kumar et al. (2022) analyzed asymmetric rolling using an energy-based upper bound framework and found a strong coupling between roll speed ratio and deformation efficiency [14].

Chen et al. (2024) also demonstrated that for advanced aluminum alloys, modified UBM formulations with continuous velocity fields offer better agreement with experimental rolling force and torque measurements [15]. The ability of slab analysis to capture asymmetric deformation behavior was established by Hwang and Tzou (1993), who derived analytical expressions for cold strip rolling under differential roll speeds [16]. The relationship between friction factor and friction coefficient was then examined by Tzou (1999), who found

frictional limits that have a direct impact on slab-method solutions [17]. Slab formulations successfully capture thickness variation and pressure distribution within the deformation zone, as shown by Gao et al.'s (2002) analysis of rolling under varying friction coefficients [18]. Slab analysis can effectively model asymmetrical sheet rolling, as demonstrated by Salimi and Kadkhodaei (2004), who also found that variations in roll speed and friction significantly change the predicted neutral plane position [19]. By using the slab method to estimate friction in asymmetric rolling, Gudur et al. (2008) showed that frictional asymmetry significantly influences roll torque and rolling force [20]. The impact of thickness reduction on roll force per unit width for various friction conditions is shown in Fig. 2.3. The roll force rises nearly linearly with reduction, highlighting how important deformation severity is. There are only slight variations in force levels when comparing unequal and equal friction coefficients. This suggests that within the examined range, reduction has a greater impact than slight friction asymmetry. The applicability of the slab method to real-world rolling operations was confirmed by Tian et al. (2009), who created slab-based pressure models for asymmetrical rolling and verified the analytical predictions using industrial rolling data [21]. Tan (2007) demonstrated that friction–velocity coupling has a significant impact on predicted rolling stress and pressure distribution by incorporating dynamic friction models into slab formulations [22]. Li et al. (2003) verified the accuracy of slab analysis in capturing velocity fields and strain distribution by using digital image correlation techniques to validate slab-based deformation predictions. [23]

Zhang et al. (2014) showed that combining sophisticated material models with slab formulations improves prediction capability by integrating the MY yield criterion with slab analysis to assess plate rolling behavior [24]. For asymmetrical rolling of large cylinders, Chen et al. (2019) developed a shear-sensitive slab model that outperformed traditional slab formulations in terms of accuracy and computational efficiency [25]. An important foundation for the current study is the sensitivity of UBM predictions to roll diameter, reduction ratio, friction factor, and back/front tension. Building on these fundamental advancements, the Upper Bound Method has been used in a number of studies to measure the impact of geometry and friction on the maximum reduction that can be achieved during strip rolling. The maximum percentage reduction is strongly dependent on the strip thickness-to-roll radius ratio (t/R_0), but it increases nonlinearly with the coefficient of friction and approaches an asymptotic limit at higher friction values, as Avitzur's classical results clearly show.

1.2 Simplifications and Assumptions for Symmetrical Rolling

The material being rolled is rigid plastic, and the roll itself is rigid. Under plane-strain conditions, plastic deformation takes place, leading to a uniform distribution of stress within the elements. The vertical and horizontal stresses are regarded as the principal stresses. Although the coefficient for the upper roll may be different from the coefficient for the lower roll, the frictional coefficients between the roll and material are constant throughout the contact arc. When material enters and leaves the roll-bite, it flows horizontally. The speed, diameter, and coefficient of friction forces applied by the upper and lower rolls are all shown in Figure 1, which illustrates the specifics of asymmetrical cold strip rolling. Depending on which way the upper and lower rolls apply friction forces to the strip, the deformation region is divided into three sections: the forward slip zone (FSZ), cross shear zone (CSZ), and backward slip zone (BSZ).

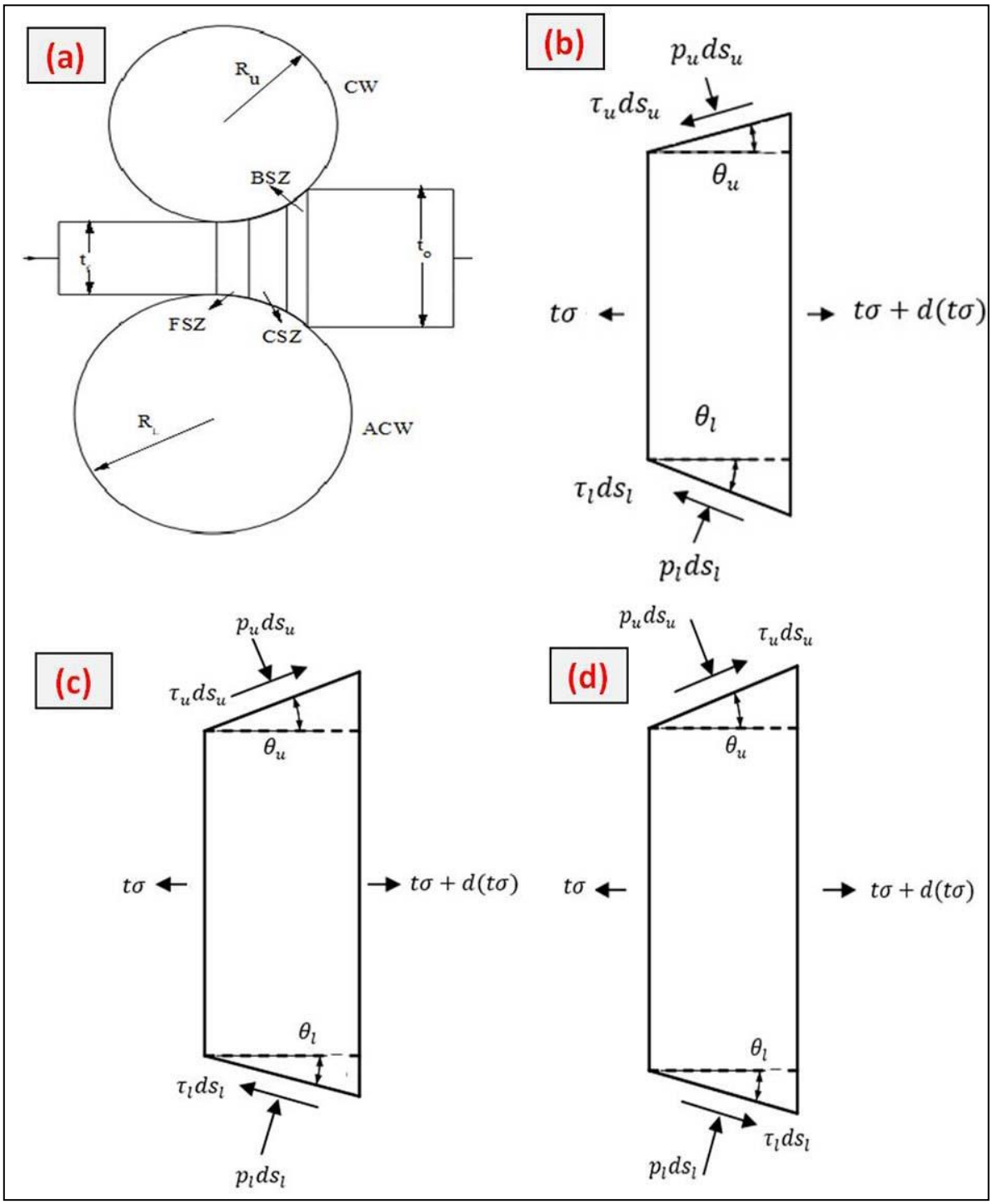

Fig. 1. (a) Schematic representation of a mathematical model (b) Element of material within Backward slip Zone (c) Element of material within cross shear Zone (d) Element of material within forward slip Zone.

a) Nomenclature:

l = length of the contact

t_u, t_l = *thickness of the upper and lower rolls*

τ_u, τ_l = *frictional stresses along the upper and lower rolls*

$p_u, p_l = specific\ roll\ pressure\ of\ \ the\ upper\ and\ lower\ rolls$

$R_u, R_l, R_{eq} = radius\ of\ \ the\ upper, lower\ and\ effective\ \ rolls$

$R_u, R_l = radius\ of\ \ the\ upper\ and\ lower\ rolls$

CW = clockwise; $ACW = anticlockwise$

$FSZ, BSZ, CSZ = forward, backward\ and\ crossward\ slip\ zones$

$\sigma, \sigma_o = horizontal\ stress, yielding\ shear\ stress\ of\ the\ material$

$\theta_u, \theta_l = Variable\ angle\ of\ contact\ of\ \ the\ upper\ and\ lower\ rolls$

$V_u, V_l = peripheral\ speed\ of\ \ the\ upper\ and\ lower\ rolls$

$\mu_u, \mu_l = peripheral\ speed\ of\ \ the\ upper\ and\ lower\ rolls$

$x_{n1}, x_{n2} = Distance\ neutral\ point\ \ of\ \ the\ upper\ and\ lower\ rolls$

$P, P_{FSZ}, P_{BSZ}, P_{CSZ} = the\ rolling\ force\ per\ unit, in\ FSZ, BSZ, CSZ\ zones$

$T_u, T_l = Rolling\ torques\ of\ upper\ and\ lower\ rolls$

b) Subscripts:

$n1, n2 = neutral\ point\ \ of\ \ the\ upper\ and\ lower\ rolls$

$u, l = \ upper\ and\ lower\ rolls$

$o = yielding\ shear\ stress$

$eff = effective\ roll\ radius$

2. Mathematical Modelling and Model Analysis

The mathematical formulations representing the equilibrium of horizontal and vertical forces are encapsulated as:

(i) Backward Slip Zone (BSZ)

$$\frac{d(t\sigma)}{dx} + p_u tan\theta_u + p_l tan\theta_l - (\tau_u + \tau_l) = 0 \quad (1)$$

$$p = p_u(1 + \mu_u tan\theta_u) = p_l(1 + \mu_l tan\theta_l) \quad (2)$$

Integrate equations one and two.

$$\frac{d(t\sigma)}{dx} + (p + \sigma)\frac{dt}{dx} = \mu_e p \quad (3)$$

The criterion for plane strain according to von Mises can be expressed as

$$p + \sigma = \frac{2}{\sqrt{3}}\sigma_0 \quad (4)$$

where $\sigma_0$represents the yielding shear stress of the material,

To substitute equation (3) and equation (4) and rearrange them

$$(1 + z^2)\frac{dF}{dz} + bF = 2z \quad (5)$$

where $b = \mu_e\sqrt{\frac{R_{eq}}{t_f}}$ $R_{eq} = \frac{2R_1R_2}{R_1 + R_2}$ $z = \frac{x}{\sqrt{R_{eq} + t_f}}$ $F = \frac{p}{\frac{2}{\sqrt{3}}\sigma_0}$

$z = \tan w$;

$$\frac{dF}{dw} + bF = 2\tan w \tag{6}$$

within the forward slip zone is stated as follows:

$$F = ce^{-bw} + \frac{2}{b}\left[\frac{w^3}{3} - \frac{w^2}{b} + sw - t\right] \tag{7}$$

where $s = 1 + \frac{2}{b^2}$; $t = \frac{1}{b} + \frac{2}{a^3}$

(ii) Forward Slip Zone (FSZ)

$$F_0 = 1 - \frac{\sigma_f}{\frac{2}{\sqrt{3}}\sigma_0} \tag{8}$$

$c_3 = F_0 + \frac{2t_3}{b_3}$ where $t_3 = \frac{1}{b_3} + \frac{2}{b_3^3}$; $s_3 = 1 + \frac{2}{b_3^2}$

the solution of the differential equation is as follows the formulation for the specific rolling pressure (F_{FSZ})

$$F_{FSZ} = \left(F_0 + \frac{2t_3}{b_3}\right)e^{-b_3 w} + \frac{2}{b_3}\left[\frac{w^3}{3} - \frac{w^2}{a_3} + s_3 w - t_3\right] \tag{9}$$

Boundary conditions**:** $x = L$ **or** $w = w_i = \tan^{-1}\frac{L}{\sqrt{[R_{eq}t_0]}}$

$$F_i = 1 - \frac{\sigma_b}{\frac{2}{\sqrt{3}}\sigma_0} c_1 = B_i e^{b_1 w_i}$$

$$F_{BSZ} = B_i e^{b_1 w_i} e^{-a_1 w} + \frac{2}{b_1}\left[\frac{w^3}{3} - \frac{w^2}{b_1} + s_1 - t_1\right] \tag{10}$$

$$t_1 = \frac{1}{b_1} + \frac{2}{b_1^3};\ B_i = F_i - \frac{2}{b_1}\left[\frac{w_i^3}{3} - \frac{w_i^2}{b_1} + s_1 w_i - t_1\right];\ s_1 = 1 + \frac{2}{b_1^2}$$

(iii) Cross Shear Zone (CSZ)

Boundary conditions:$x = x_{n2}$

Due to the continuity of the boundary conditions at

$$c_2 = c_3 e^{B_1 w_{n2}} + e^{a_2 w_{n2}}(B_2 w_{n2}^3 - B_3 w_{n2}^2 + B_4 w_{n2} - B_5)$$

where $B_1 = a_2 - a_3$, $B_2 = \frac{2}{3a_3} - \frac{2}{3a_2}$ $B_3 = \frac{2}{3a_3^2} - \frac{2}{a_2^2}$

$$B_4 = \frac{2s_3}{a_3} - \frac{2s_2}{a_2} B_5 = \frac{2t_3}{a_3} - \frac{2t_2}{a_2}$$

from the constancy of volume, the position of the upper and lower neutral points x_{n1}, x_{n2}

$$x_{n1} = R_1\sqrt{V_A\frac{x_{n2}^2}{R_1^2} + (V_A - 1)\frac{t_b}{R_A}} \text{ where } V_A = \frac{V_l}{V_u}, R_A = \frac{R_1}{2}\left(1 + \frac{R_1}{R_2}\right)$$

(iv) Rolling Force

The rolling force per unit width is given by integrating the normal rolling pressure over the arc length of contact once the yielding stress and coefficient of friction are known.

$$P = P_{FSZ} + P_{CSZ} + P_{BSZ} \tag{11}$$

$$P_{FSZ} = \frac{2}{\sqrt{3}}\sigma_0 \int_0^{Xn2} F_{FSZ}\,dx = \frac{2}{\sqrt{3}}\sigma_0\sqrt{R_{eq}t_0}\left(F_{FSZ_1} + F_{FSZ_2}\right) \quad (12)$$

$$F_{FSZ_1} = \frac{-c_3 e^{-a_3 w_{n2}}}{a_3}\left(1 + w_{n2}^2 + \frac{2w_{n2}}{a_3} + \frac{2}{a_3^2}\right) + \frac{c_3}{a_3} + \frac{2c_3}{a_3^3}$$

$$F_{FSZ_2} = \frac{w_{n2}^6}{9a_3} - \frac{2w_{n2}^5}{5a_3^2} + \frac{\frac{1}{3}+s_3}{2a_3}w_{n2}^4 - \frac{2}{3a_3}\left(\frac{1}{a_3}+t_3\right)w_{n2}^3 + \frac{s_3 w_{n2}^2}{a_3} - \frac{2t_3 w_{n2}}{a_3}$$

$$P_{CSZ} = \frac{2}{\sqrt{3}}\sigma_0 \int_0^{Xn2} F_{CSZ}\,dx = \frac{2}{\sqrt{3}}\sigma_0\sqrt{R_{eq}t_0}\left(F_{CSZ_1} + F_{CSZ_2}\right) \quad (13)$$

$$F_{CSZ_1} = \frac{-c_2 e^{-a_2 w_{n1}}}{a_2}\left(1 + w_{n1}^2 + \frac{2w_{n1}}{a_2} + \frac{2}{a_2^2}\right) + \frac{w_{n1}^6}{9a_2} - \frac{2w_{n1}^5}{5a_2^2} + \frac{\frac{1}{3}+s_2}{2a_2}w_{n1}^4 - \frac{2}{3a_2}\left(\frac{1}{a_2}+t_2\right)w_{n1}^3 + \frac{s_2}{a_2}w_{n1}^2 - \frac{2t_2}{a_2}w_{n1}$$

$$F_{CSZ_2} = \frac{-c_2 e^{-a_2 w_{n2}}}{a_2}\left(1 + w_{n2}^2 + \frac{2w_{n2}}{a_2} + \frac{2}{a_2^2}\right) - \frac{w_{n1}^6}{9a_2} - \frac{2w_{n2}^5}{5a_2^2} - \frac{\frac{1}{3}+s_2}{2a_2}w_{n2}^4 + \frac{2}{3a_2}\left(\frac{1}{a_2}+t_2\right)w_{n2}^3 - \frac{s_2}{a_2}w_{n2}^2 + \frac{2t_2}{a_2}w_{n2}$$

$$P_{BSZ} = \frac{2}{\sqrt{3}}\sigma_0 \int_0^{L} F_{BSZ}\,dx = \frac{2}{\sqrt{3}}\sigma_0\sqrt{R_{eq}t_0}\left(F_{BSZ_1} + F_{BSZ_2}\right) \quad (14)$$

Where:

$$F_{BSZ_1} = \frac{-c_1 e^{-a_1 w_i}}{a_1}\left(1 + w_i^2 + \frac{2w_i}{a_1} + \frac{2}{a_1^2}\right) + \frac{w_i^6}{9a_1} - \frac{2w_i^5}{5a_1^2} + \frac{\frac{1}{3}+s_1}{2a_1}w_i^4 - \frac{2}{3a_1}\left(\frac{1}{a_1}+t_1\right)w_i^3 + \frac{s_1}{a_1}w_i^2 - \frac{2t_1}{a_1}w_i$$

$$F_{BSZ_2} = \frac{-c_1 e^{-a_1 w_{n1i}}}{a_1}\left(1 + w_{n1}^2 + \frac{2w_{n1}}{a_1} + \frac{2}{a_1^2}\right) - \frac{w_{n1}^6}{9a_1} + \frac{2w_{n1}^5}{5a_1^2} - \frac{\frac{1}{3}+s_1}{2a_1}w_{n1}^4 + \frac{2}{3a_1}\left(\frac{1}{a_1}+t_1\right)w_{n1}^3 - \frac{s_1}{a_1}w_{n1}^2 + \frac{2t_1}{a_1}w_{n1}$$

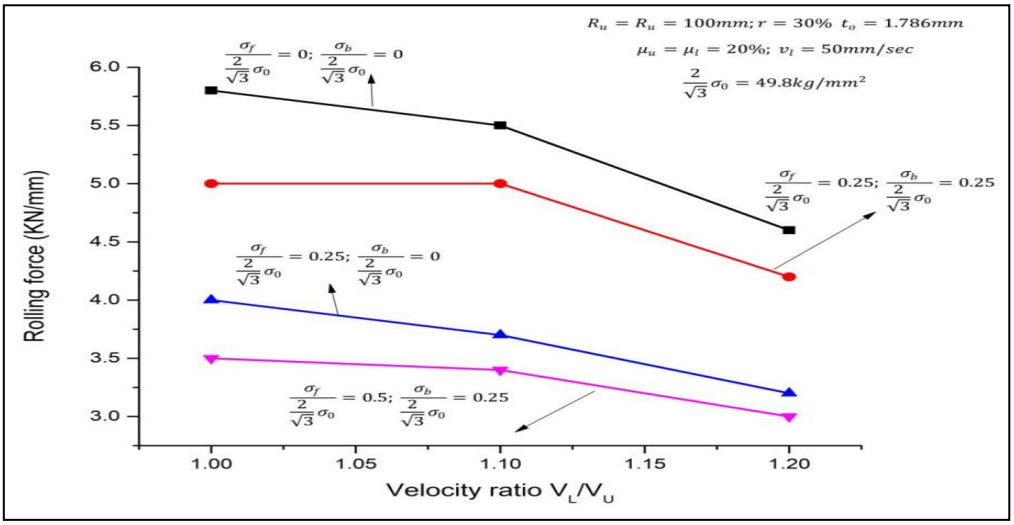

Fig. 2. For various front and back tensions, variations of rolling force with roll speed ratio

Each curve in Figure 2 represents a particular set of frictional stress conditions that are normalized by the yielding stress. The rolling process without any frictional stresses on the material is represented by the first curve. The rolling force slightly decreases as the velocity ratio rises. As the upper and lower roll speeds get closer to equality, this decrease is explained by a more balanced rolling condition. In comparison to the first curve for the same velocity ratio, the second curve illustrates the impact of adding forward frictional stress with a 25% reduction in rolling force. When rolling, forward friction helps to lessen resistance. Forward and backward frictional stresses acting equally are represented by the third curve. In comparison to the second curve, rolling force is further decreased. This suggests that when friction is balanced in both forward and backward directions, rolling conditions are more favorable. The effect of greater forward friction in comparison to backward friction is shown by the fourth curve: Out of all the cases, rolling force is the least. Increased forward friction greatly facilitates material deformation and lowers the rolling force needed. As the velocity ratio rises, rolling force falls. Compared to backward frictional stress, forward frictional stress more successfully lowers the rolling force. Rolling force is moderately reduced when forward and backward stresses are balanced, as in the third curve. The rolling process is optimized when there is less backward friction and more forward friction (as in the fourth curve), which reduces the rolling force. The rolling force and pressure distribution are influenced by contact length. The deformation zones (FSZ, BSZ, and CSZ) are affected by roll pressure. Points that are neutral. The places where roll surface velocity and material velocity coincide.

(v) Rolling Torque

Therefore, the rolling torque T_u and T_l exerted by the strip on the upper and lower rolls, respectively, can be calculated by integrating the moment of the frictional force along the arc of contact about the roll axis.

$$T_u = R_u(\mu_u P_{BSZ} - \mu_u P_{CSZ} - \mu_u P_{FSZ}) \quad (15)$$

$$T_l = R_l(\mu_l P_{BSZ} - \mu_l P_{CSZ} - \mu_l P_{FSZ}) \quad (16)$$

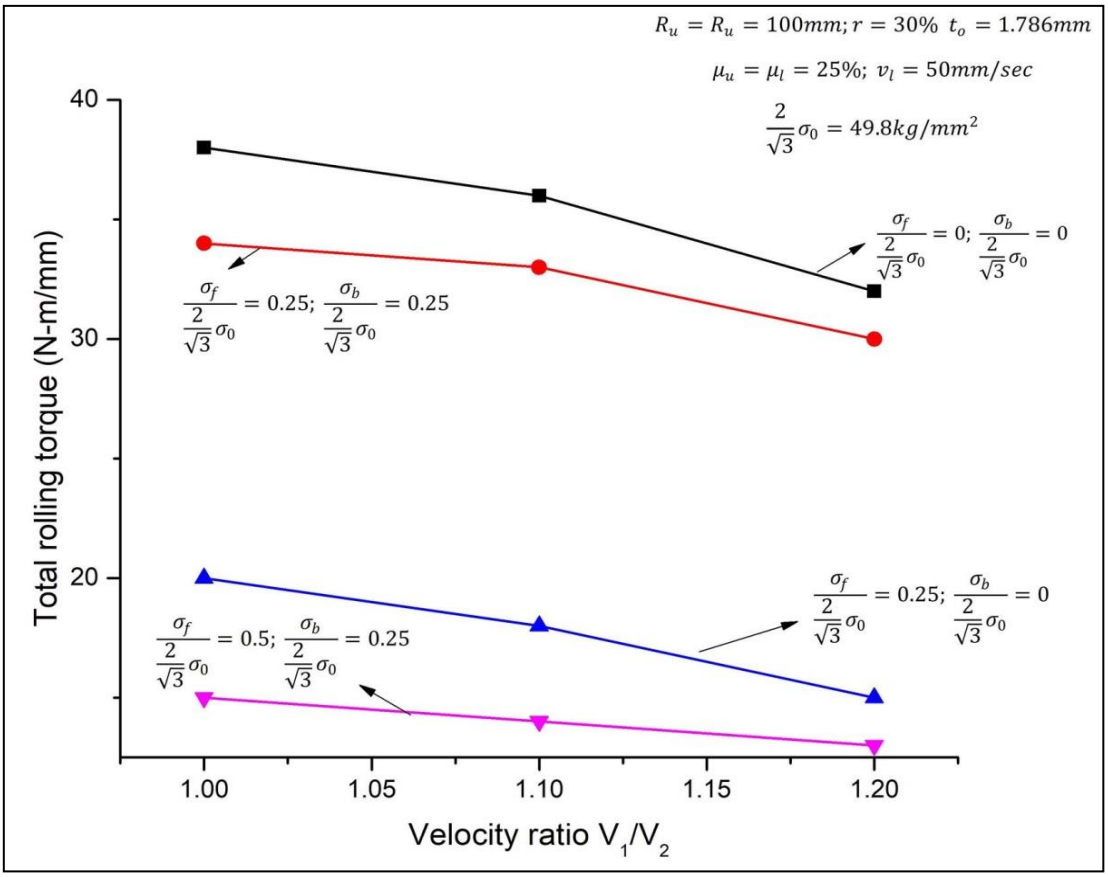

Fig. 3. For various front and back tensions, variation of rolling torque with roll speed ratio.

The curves in Figure 3 are as follows: A frictionless rolling situation with no forward or backward frictional stresses is depicted by the first curve. In this instance, as the velocity ratio rises, the overall rolling torque falls. However, the torque requirements are higher than in other scenarios because there is no friction. Balanced forward and backward frictional stresses are represented by the second curve. Similar to the black curve, torque decreases as the velocity ratio increases, but because friction helps in both directions, the torque is lower. The third curve excludes backward friction and only includes forward frictional stress. In contrast to the second curve, there is less rolling torque. Both resistance and the torque needed to deform the material are decreased by forward friction. The fourth curve depicts a situation with moderate backward friction and increased forward friction. For every velocity ratio, this curve shows the lowest torque values. Increased forward friction greatly facilitates material flow, lowering torque and rolling resistance.

The torque distribution along the roll surfaces is influenced by the contact length. Because they delineate areas of slip and no-slip, neutral points have an impact on torque behavior. Roll Radii Higher torques are usually associated with larger radii.

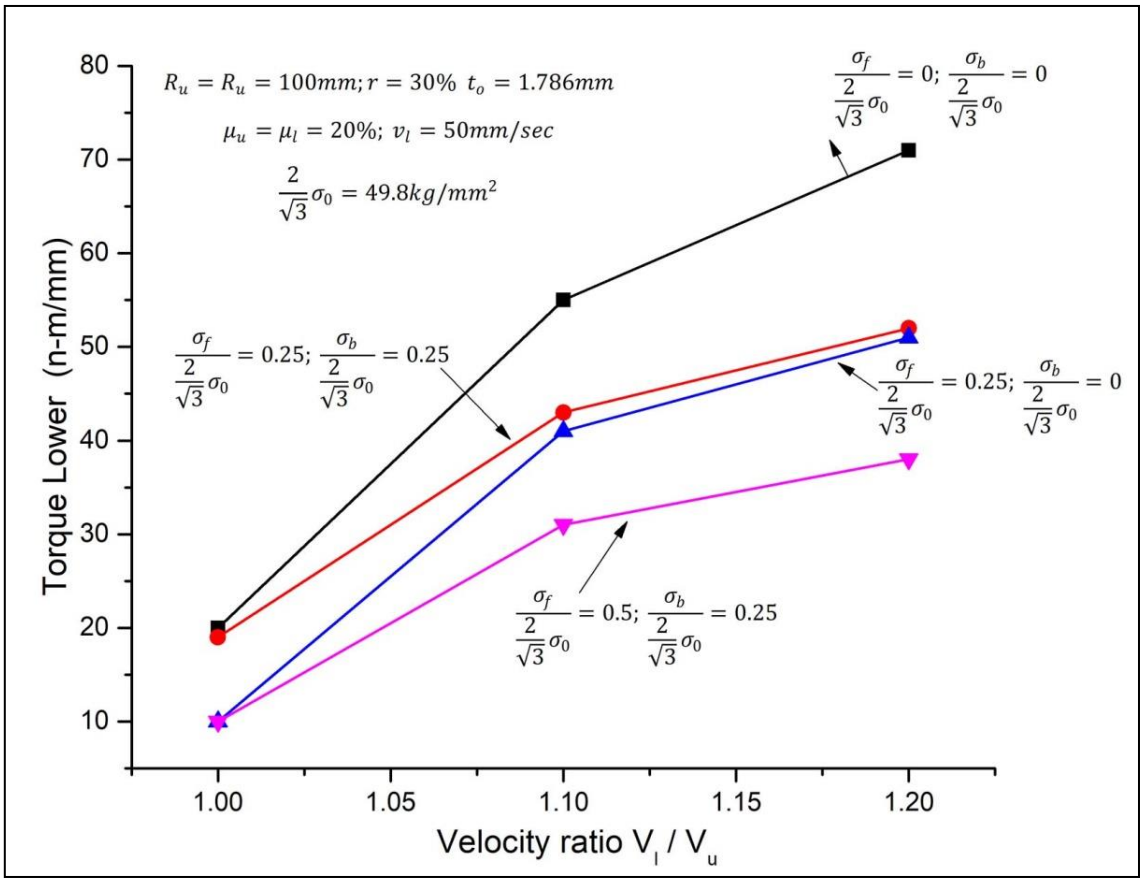

Fig. 4. Variation of high-speed rolling torque with roll speed ratio for various front and rear tensions

The curves in Figure 4 are as follows: the first curve shows a rolling state in which there are no forward or backward tensions. As the velocity ratio rises, the torque on the lower roll increases dramatically. When there are no tension stresses, more torque is needed than in other situations. Forward and backward tensions are balanced in the second curve. Although it is less than the first curve, the torque rises with the velocity ratio. By dispersing stresses uniformly throughout the roll interface, balanced tensions aid in lowering torque requirements. Forward tension without any backward tension is represented by the third curve. Since forward tension facilitates the material's deformation and lowers resistance, the torque is further reduced when compared to the red curve. The fourth curve indicates a state with moderate backward tension and increased forward tension. For every velocity ratio, this curve shows the lowest torque values. The least amount of torque is needed when forward tension is increased because it greatly lowers resistance. In every scenario, the torque on the lower roll rises as the velocity

ratio does. When low or moderate backward tension is paired with higher forward tension, less torque is needed, improving rolling conditions.

In comparison to situations that favor higher forward tension, balanced forward and backward tensions (second curve) provide a moderate torque reduction. The torque is highest when there are no tension stresses (first curve), indicating more rolling resistance. The torque needed for deformation is influenced by the contact length. The torque behavior and stress distribution are influenced by the friction coefficient. The areas of slip and the torque that results from them are determined in part by neutral points. Tension Distribution: While backward tension impacts the backward slip zone (BSZ), forward tension lowers resistance in the forward slip zone (FSZ).

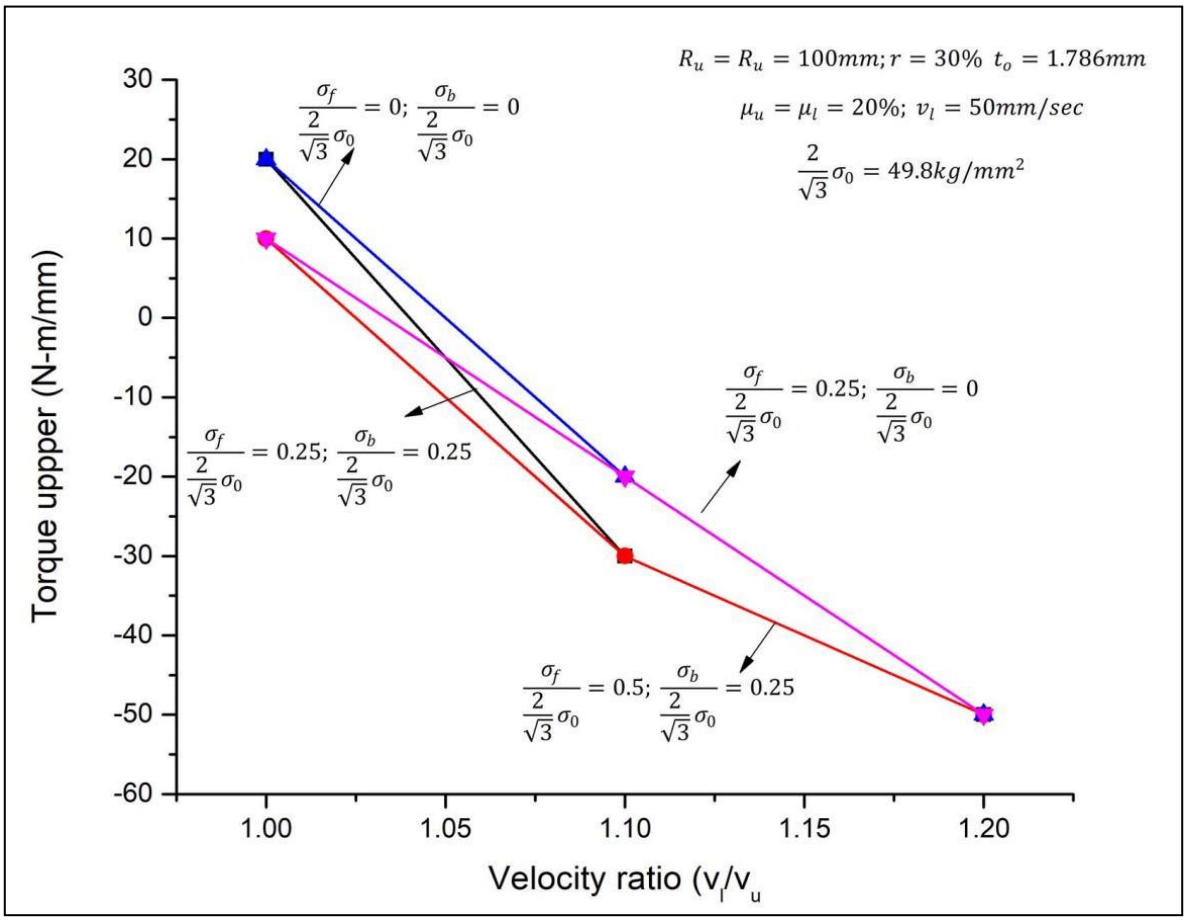

Fig. 5. For various front and back tensions, variations of low-speed rolling torque with roll speed ratio

The curves in Figure 4 are as follows: Rolling without any forward or backward tension stresses is represented by the first curve. As the velocity ratio rises, the upper roll torque gradually decreases. When frictional tensions are absent, torque magnitudes are comparatively higher than under other circumstances. A balanced rolling scenario with equal forward and backward tension stresses is represented by the second curve. Although it is less negative than the first curve, the torque on the upper roll decreases with the velocity ratio. Lower torque values are needed because balanced tensions lower resistance. Forward tension without any backward tension is represented by the third curve. In comparison to the second curve, the torque reduction is more substantial. Torque magnitudes are further reduced by forward tension, which lowers resistance in the forward slip zone. The fourth curve represents rolling with a moderate backward tension and a higher forward tension. The largest decrease in upper roll torque is seen in the fourth curve. The least amount of torque is needed when forward tension is increased because it reduces resistance.

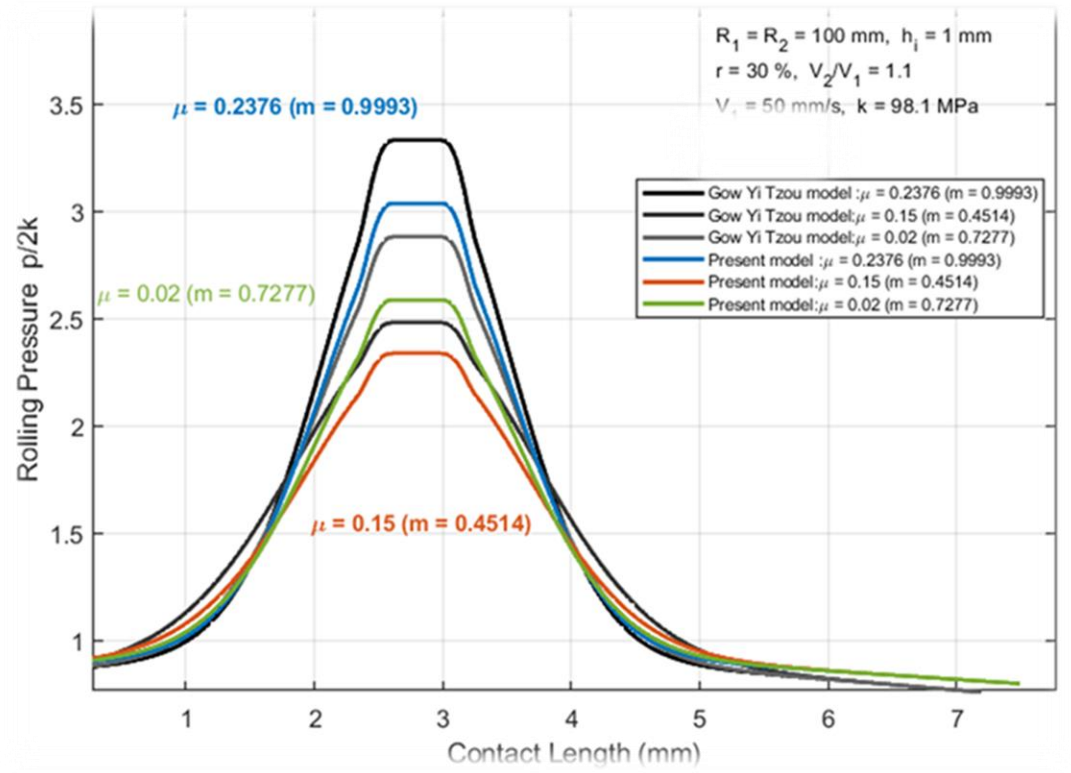

Fig. 6. Rolling pressure distributions along the contact length for various friction coefficients at a fixed reduction of 30%, as compared by the Gow Yi Tzou model with present model

2.1 The Upper Bound Approach to Plane of Velocity Interruption

The plane of velocity interruption among the adjacent bodies subjected to rotational resistant bodies Assume an arbitrary plane of velocity interruption S having an orientation of the normal components of velocity are equal

$$normal\ components\ of\ velocity\ are\ equal$$

$$r_i\omega_i\, cos(\beta_o - \psi) = r_j\omega_j\, cos(\psi - \beta_o)$$

$$r_i\omega_i(cos\,\beta_o\ - sin\,\beta_o\ tan\,\psi) = r_j\omega_j(\ cos\,\beta_o - tan\,\psi\ \ sin\,\beta_o)$$

$$r_i\omega_i(cos\,\beta_o\ \ cos\,\psi - sin\,\beta_o\ \ sin\,\psi) = r_j\omega_j(cos\,\psi\ \ cos\,\beta_o - sin\,\psi\ \ sin\,\beta_o)$$

$$tan\,\psi = \frac{sin\,\psi}{cos\,\psi} = \frac{(x - x_c)}{\sqrt{0.5D^2 - (x - x_c)^2}}$$

$$\left(x - \frac{x_{0i} - \xi\ x_{0j}}{1 - \xi}\right)^2 + \left(y - \frac{y_{0i} - \xi\ y_{0j}}{1 - \xi}\right)^2 = \frac{2C\omega}{1 - \xi} + \left(\frac{x_{0i} - \xi\ x_{0j}}{1 - \xi}\right)^2 + \left(\frac{y_{0i} - \xi\ y_{0j}}{1 - \xi}\right)^2 \left(\because \xi = \frac{\omega_j}{\omega_i}\right)$$

$$the\ \ \rightleftarrows\rightleftarrows\ velocity\ in\ terruption$$

$$\Delta u = u_{iT} - u_{jT} = u_i\, sin(\beta_o - \psi)\ + u_j\, sin(\psi - \beta_o)$$

$$\Delta u = \left(\frac{1}{0.5D}\right)\begin{bmatrix}\omega_i(y - y_{0i})(y - y_c) - \omega_i(x - x_{0i})[-(x - x_c)] + \omega_j(x - x_{0j}) \\ +[-(x - x_c)] - \omega_j(y - y_{0j})(y - y_c)\end{bmatrix}$$

$$\Delta u = \ 0.5D\left|\omega_i\left(1 - \frac{\omega_j}{\omega_i}\right)\right| \quad = 0.5D|\omega_i(1 - \tau)|$$

$$\varphi_{EF} = 2\ sin^{-1}\frac{\overline{EF}}{D} = 2\,sin^{-1}\sqrt{\frac{(x_E - x_F)^2 + (y_E - y_F)^2}{D}}$$

$$\overline{EF} = D\left(\pi - sin^{-1}\sqrt{\frac{(x_E - x_F)^2 + (y_E - y_F)^2}{D}}\right)$$

Shear power losses along the velocity of plane when the both resistant bodies are in rotational

$$P_s = \int_S \frac{\sigma_o}{\sqrt{3}} D|\omega_i(1-\xi)|\ \overline{EF}$$

$$P_s = \int_S \frac{\sigma_o}{\sqrt{3}} D|\omega_i(1-\xi)|\ D\left(\pi - sin^{-1}\sqrt{\frac{(x_E - x_F)^2 + (y_E - y_F)^2}{D}}\right)$$

Shear power losses along the velocity of plane when the both resistant bodies are in translations

$$tan\,\theta_i = -\frac{(x - x_{0i})}{(y - y_{0i})} \qquad tan\,\theta_j = -\frac{(x - x_{0j})}{(y - y_{0j})}$$

$$tan\,\psi = \frac{tan\,\theta_i\,(y - y_{0i}) - \xi\,tan\,\theta_j\,(y - y_{0j})}{(y - y_{0i}) - \xi(y - y_{0j})} \left(\because \xi = \frac{\omega_j}{\omega_i}\right)$$

$$\xi = \tau\frac{cos\,\theta_j}{cos\,\theta_i}\left[\frac{(y - y_{0i})}{(y - y_{0j})}\right] = \tau\frac{sub\theta_j}{sin\,\theta_i}\left[\frac{(x - x_{0i})}{(x - x_{0j})}\right]\left[\because \tau = \frac{u_j}{u_i}\right]$$

$$\Delta u = u_i\sqrt{1 + \tau^2 - 2\tau\,cos\,\varphi}$$

$$P_s = \int_S \frac{\sigma_o}{\sqrt{3}}\frac{\Delta u^2 dx}{u_i(cos\,\theta_i - \tau\,cos\,\theta_j)} = \frac{\sigma_o}{\sqrt{3}}\frac{\Delta u^2(x_E - x_F)}{u_i(cos\,\theta_i - \tau\,cos\,\theta_j)}$$

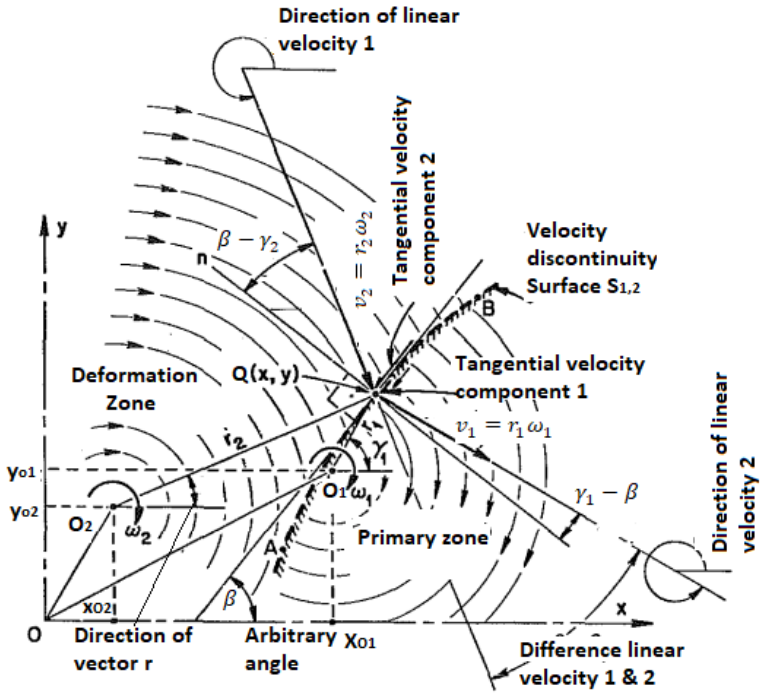

Fig. 7. Two rigid bodies in rotational motion-boundary of velocity discontinuity

(Courtesy: Betzalel Avitzur Professor and Director, Insitutue for Metal Forming, Department of Metallurgy and Materials Engineering, Lehigh niversity, Bethlehem, Pa. 18015)

$$v_1 cos(\gamma_1 - \beta) = v_2 cos(\beta - \gamma_2) \tag{17a}$$

$$v_1 cos\gamma_1 - v_1 sin\gamma_1 \frac{dy}{dx} = v_2 cos\gamma_2 - v_2 sin\gamma_2 \frac{dy}{dx} \tag{17b}$$

$$\int \frac{dy}{dx} dx = \int \left(\frac{v_2 cos\gamma_2 - v_1 cos\gamma_1}{v_2 sin\gamma_2 - v_1 sin\gamma_1}\right) dx \tag{17c}$$

$$(x - X)^2 + (y - Y)^2 = \frac{C_1 \omega_1}{1-\lambda} + (X)^2 + (Y)^2 \tag{17d}$$

$where\ \ X = \frac{x_{01} - \lambda x_{02}}{1-\lambda}; Y = \frac{y_{01} - \lambda y_{02}}{1-\lambda}; C_1 = constat\ of\ integration$

2.2 An Upper Bound Approach for Power Analysis of Cold Strip Rolling

B. Avitzur et.al,[1] conducted experimental work and develop the model to calculate the separation force, the minimum power requirement and coefficient of friction for the mises material dimensionless parameter identified and it is proportionally increase with the maximum possible reduction, maximum percentage reduction was effected by the process variables like coefficient of friction standard unit. Assumed stress distribution:

1. Separation Force P

The separation force is directly formulated based on stress variation according to the experimental detail, it shows that if the roll separation force with no tensions is achieved experimentally then, the accurate value of the separating force can be achieved.

$$P = \frac{2}{3}\sigma_o \sqrt{R_o(t_i - t_f)} * \left[1 - \frac{1}{2} \frac{\sigma_{xf} + \sigma_{xb}}{\frac{2}{3}\sigma_o}\right]$$

2. Roll Power WR:

if thefriction coefficient greater than the min value and the position of the neutral point moves towards the exit then the velocity of the exit is reduced and the requirement of power for deformation falls, if the friction coefficient equal to its minimum value the outlet velocity does not influence the power equilibrium

$$\dot{W}_R = \frac{2}{\sqrt{3}}\sigma_o UQ * t_f \sqrt{\frac{t_i}{t_f} - 1} * \quad K - \frac{2}{3}\frac{\sigma_{xb} - \sigma_{xf}}{\frac{2}{\sqrt{3}}\sigma_o}$$

3. Torque T

$$T = \frac{2}{\sqrt{3}}\sigma_o Q(R_o t_f) \sqrt{\frac{t_i}{t_f} - 1} \quad * K - \frac{2}{3}\frac{\sigma_{xb} - \sigma_{xf}}{\frac{2}{\sqrt{3}}\sigma_o}$$

4. Position of the Neutral Point (when αn =0)

for any percentage decrease under some possible condition, the friction coefficient and be high, if friction coefficient crosses its minimum value then the position of the neutral point changes form exit to entry, if it is continue i.e., greater friction coefficients the position of the neutral point moves near to the entrance, at the same time the exit velocity will rise.

$$2Q = \frac{ln\frac{t_i}{t_f} + \frac{\sigma_{xb} - \sigma_{xf}}{\frac{2}{\sqrt{3}}\sigma_o}}{\frac{\sigma_{xb} - \sigma_{xf}}{\frac{2}{\sqrt{3}}\sigma_o \sqrt{\frac{t_i}{t_f} - 1}} \left[ln\left\{\frac{\sqrt{t_i - t_f}}{t_n}\right\} + \left(\frac{\sigma_{xb}}{\frac{2}{\sqrt{3}}\sigma_o} - 1\right)\right] * 2\ tan^{-1}\sqrt{\frac{R_o}{t_f}}\alpha_n - tan\sqrt{\frac{t_i}{t_f} - 1}}$$

5. Torque (when αn =0)

$$T = \frac{2}{\sqrt{3}}\sigma_o Q(R_o t_f)\sqrt{\frac{t_i}{t_f}-1}\left[1-\frac{1}{2}\frac{\sigma_{xb}-\sigma_{xf}}{\frac{2}{\sqrt{3}}\sigma_o}\right]$$

According to Whitton's experimental data the Separation force and the Torque formulations as follows

$$P = B_o + B_1\left(\sigma_o\sqrt{t_i - t_f}_{\ f}\right) + B_2\left(\sigma_{xb}\sqrt{t_i - t_f}\right)$$

$$T = A_o + A_1\left(\sigma_o\mu\sqrt{t_i - t_f}_{\ f}\right) + A_2\left(\sigma_{xb}\mu\sqrt{t_i - t_f}\right)$$

2.3 An Upper Bound Approach Using Kinematically Admissible Velocity Fields (KAVF) and Kinematical Admissible Strain Rate Field (KASRF) in Cold-Strip Rolling

Betzalel et al [2] Determine actual work done by the rolling by assuming the coulomb friction and shear stress experimental results are analysed and derived the mathematical expression for power consumption, shear stress, efficiency, minimum friction, maximum reduction, neutral point position finally the impact has been observed on the energy consumption. and also the influence of variables on power consumption has been observed.

1. Upper Bound on Energy Consumption:

The contact plane between stock and the rollers was assumed as a velocity discontinuity and uniform shear stress also the columb friction between rolls and stock. Kinematically admissible velocity field is which executes the uniform density whole the body and extreme conditions on the surface. Kinematically admissible strain rate field (KASRF) is originated from a KAVF, the upper bound energy utilization is translated to the influence that the energy given by the roll power is same the roll power of elongation is consumed only in deformation zone.

$$J^* = K\sqrt{2}\int_{(v)}\sqrt{\dot{\varepsilon}_{ij}\dot{\varepsilon}_{ij}}\,dV - \int_{s_i}\tau_i\, v_i * ds$$

2. Pressure of Rolls on Strip

let the uniform pressure variation be selected, friction hill effect and roll flattening were omitted then the pressure of rollers on stock is given by the formulation given apart the uniform pressure variation and length of arc contact and friction coefficient were considered.

$$P = \frac{2}{3}\sigma_o\left[1-\frac{1}{3}\frac{\sigma_{xf}-2\sigma_{xb}}{\frac{2}{\sqrt{3}}\sigma_o}\right]$$

Average Pressure with stone's the approximations is significant for nominal reductions and mean front and back tensions.

$$P = \frac{2}{3}\sigma_o\left(1-\frac{1}{3}\frac{\sigma_{xf}-2\sigma_{xb}}{\frac{2}{\sqrt{3}}\sigma_o}\right)\frac{Exp\left(\frac{\mu L}{t_o}\right)-1}{\frac{\mu L}{t_o}}$$

$$t_o = \frac{t_i+t_f}{2} \quad L = \sqrt{R_o(t_i - t_f) + \left[\frac{8R_o(1-\upsilon^2)}{\pi E}p\right]^2} + \frac{8R_o(1-\upsilon^2)}{\pi E}p$$

3. Minimum Energy Required

As you know the external power is transferred to the stock through the friction, the power required is optimized if the rolling is done with minimum shear factor when the position of the neutral point is at the exit.

$$J^* = \frac{2}{\sqrt{3}}\sigma_o U t_f \frac{\sqrt{\frac{t_i}{t_f}-1}}{tan^{-1}\sqrt{\frac{t_i}{t_f}-1}}\left[ln\frac{t_i}{t_f} + \frac{1}{4}\sqrt{\frac{t_i}{R_o}}\sqrt{\frac{t_i}{t_f}-1} + \frac{\sigma_{xb}-\sigma_{xf}}{\frac{2}{\sqrt{3}}\sigma_o}\right]$$

4. Efficiency

The efficiency factor is defined as the ratio of power of internal deformation to work required per unit volume, the efficiency factor is inversely proportional to the percentage reductions for moderate reductions such as 10-20 % the efficiency factor is high, for higher reductions the efficiency factor is low.

$$\xi = \frac{W_i}{W}$$

$$W = \frac{\frac{2}{\sqrt{3}}\sigma_o}{1+\frac{R_o}{t_f}\alpha_n^2}\left\{ln\frac{t_i}{t_f} + \frac{1}{4}\sqrt{\frac{t_i}{R_o}}\sqrt{\frac{t_i}{t_f}-1} + \frac{\sigma_{xf}-\sigma_{xb}}{\frac{2}{\sqrt{3}}\sigma_o}\frac{R_o}{t_f}\alpha_n^2 + \frac{m}{\sqrt{\frac{t_f}{R_o}}}\left[\sqrt{\frac{t_i}{t_f}-1} - tan^{-1}\sqrt{\frac{t_i}{t_f}-1}\right]\right\}$$

$$W_i = \frac{2}{\sqrt{3}}\sigma_o\, ln\frac{t_i}{t_f}$$

2.4 An Upper Bound Approach to Calculate of Roll Power and Friction Coefficient in Cold Strip Rolling with Tensions

The roll power for internal deformation is given by

$$W_i = \frac{2}{3}v_f t_f\left\{\left[\sigma_{oi} + \frac{\sigma_{of}-\sigma_{oi}}{t_i-t_f}t_i\right]ln\frac{t_i}{t_f} - (\sigma_{of}-\sigma_{oi})\right\} \quad (18)$$

W_i=Internal power of deformation

1. Co-efficient of Friction

The friction coefficient is one process parameter which influencing the maximum percentage reduction the friction coefficient function of many process parameters such as surface roughness of the roller and stock, speed of the rollers and lubricants used to check the various conditions for maximum reductions with 20-inch roller diameter and the coefficient of friction 7%/

$$\mu = \frac{1}{2}\sqrt{\frac{t_f}{R_o}}\frac{\left[\sigma_{oi}+\frac{\sigma_{of}-\sigma_{oi}}{t_i-t_f}t_i\right]ln\frac{t_i}{t_f} - (\sigma_{of}-\sigma_{oi}) + \frac{\sigma_{xb}-\sigma_{xf}}{\frac{2}{\sqrt{3}}}}{\frac{\sqrt{3}}{2}(\sigma_{xb}-\sigma_{xf})-(\sigma_{of}-\sigma_{oi})}}{\sqrt{\left(\frac{t_i}{t_f}-1\right)-\left\{\frac{\sqrt{3}}{2}\left[\sigma_{xb}+\frac{\sigma_{xf}-\sigma_{xb}}{t_i-t_f}t_i\right]-\left[\sigma_{oi}+\frac{\sigma_{of}-\sigma_{oi}}{t_i-t_f}t_i\right]\times tan^{-1}\sqrt{\left(\frac{t_i}{t_f}-1\right)}\right\}}}$$

2.5 An Upper Bound Approach to Maximum Reduction in Cold Strip Rolling

The equation for power balance:

$$2(W_R - W_F) = W_i + W_b - W_a$$

W_i=Internal power of deformation W_a= Power Introduced by The front pull

W_b= Power Deducted By the back pull W_f=Frictional Power losses

$$W_i = \frac{2}{3}v_f t_f\left\{\left[\sigma_{oi} + \frac{\sigma_{of}-\sigma_{oi}}{t_i-t_f}t_i\right]ln\frac{t_i}{t} - (\sigma_{of}-\sigma_{oi})\right\}$$

$$W_a = \sigma_{xf}\ t_f\ U$$

$$W_b = \sigma_{xb}\ t_f\ U \quad W_R - W_f$$

$$= -\frac{2}{\sqrt{3}}\sigma_o\sqrt{(R_o t_f)}\ \mu U\left\{\left[\frac{\sigma_{xb}+\frac{\sigma_{xf}-\sigma_{xb}}{t_i-t_f}t_i}{\frac{2}{\sqrt{3}}\sigma_o}-1\right]tan^{-1}\sqrt{\left(\frac{t_i}{t_f}-1\right)}-\frac{\sigma_{xf}-\sigma_{xb}}{\frac{2}{\sqrt{3}}\sigma_o\sqrt{\left(\frac{t_i}{t_f}-1\right)}}\right\} \quad (19)$$

coefficient of friction

$$\mu=\frac{1}{2}\sqrt{\frac{t_f}{R_o}}\frac{\left[\sigma_{oi}+\frac{\sigma_{of}-\sigma_{oi}}{t_i-t_f}t_i\right]ln\frac{t_i}{t_f}-(\sigma_{of}-\sigma_{oi})+\frac{\sigma_{xb}-\sigma_{xf}}{\frac{2}{\sqrt{3}}}}{\frac{\sqrt{3}}{2}(\sigma_{xb}-\sigma_{xf})-(\sigma_{of}-\sigma_{oi})}{\sqrt{\left(\frac{t_i}{t_f}-1\right)-\left\{\frac{\sqrt{3}}{2}\left[\sigma_{xb}+\frac{\sigma_{xf}-\sigma_{xb}}{t_i-t_f}t_i\right]-\left[\sigma_{oi}+\frac{\sigma_{of}-\sigma_{oi}}{t_i-t_f}t_i\right]\times tan^{-1}\sqrt{\left(\frac{t_i}{t_f}-1\right)}\right\}}} \quad (20)$$

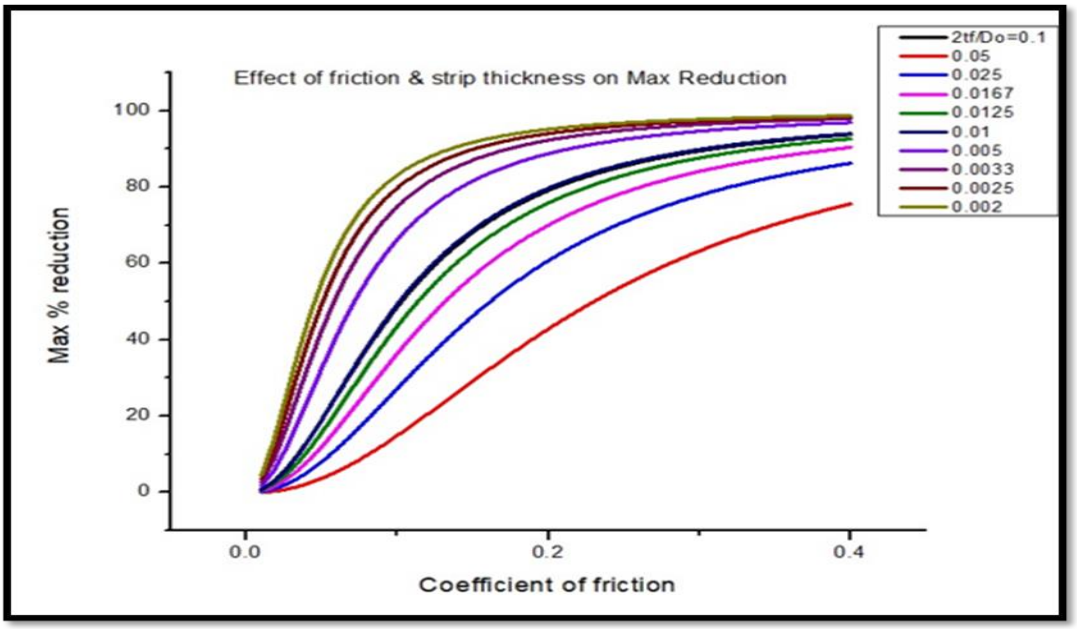

Fig. 7. Effect of front load on the minimum coefficient of friction

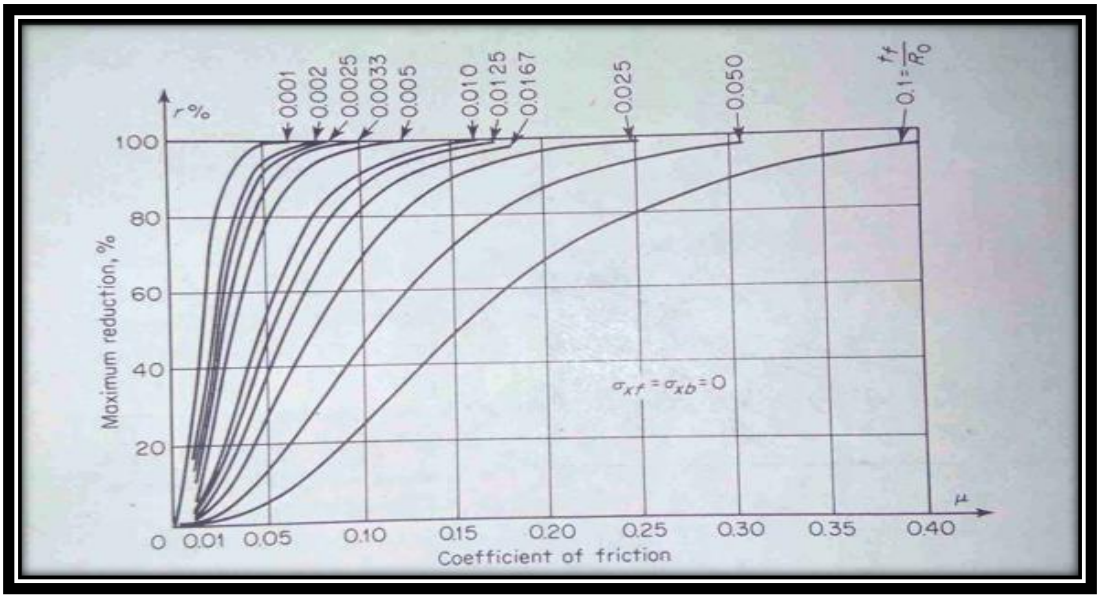

Fig. 8. Effect of friction and strip thickness (tf /Ro) on maximum reduction

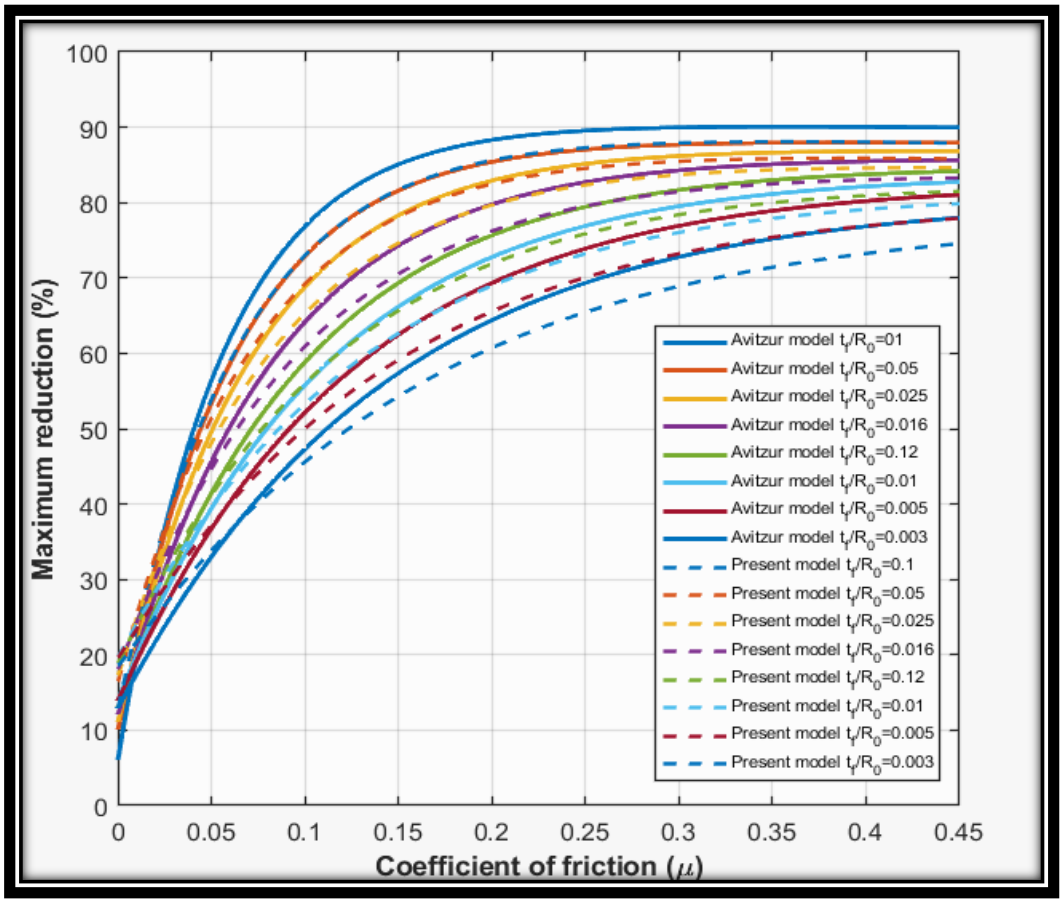

Fig. 9. Effect of maximum reduction vs coefficient of friction

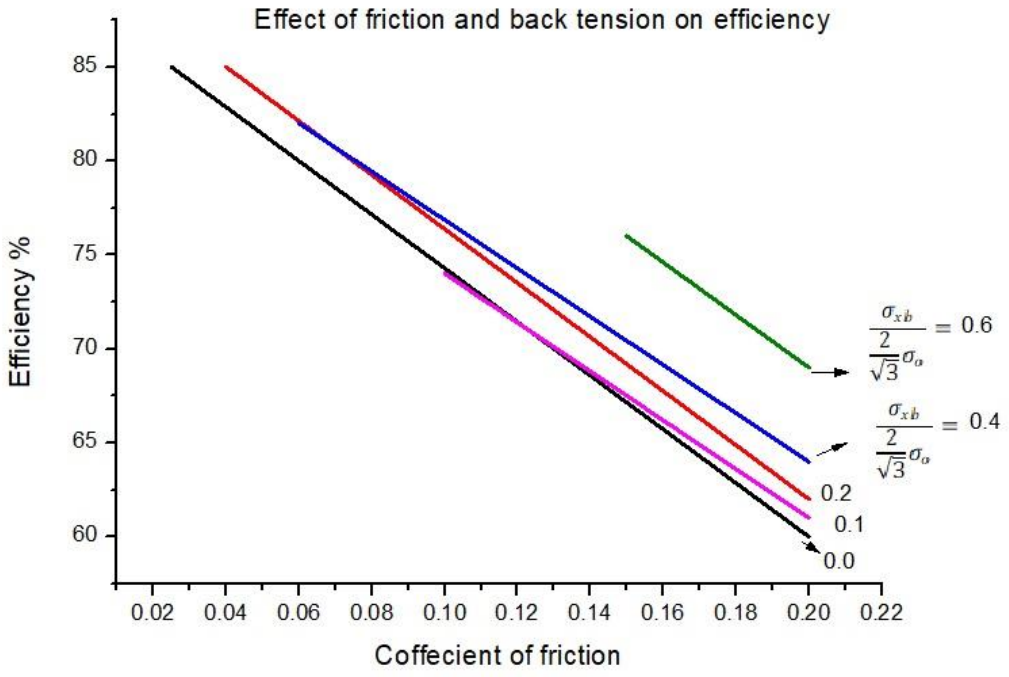

Fig. 10. Effect of friction and back tension on efficiency

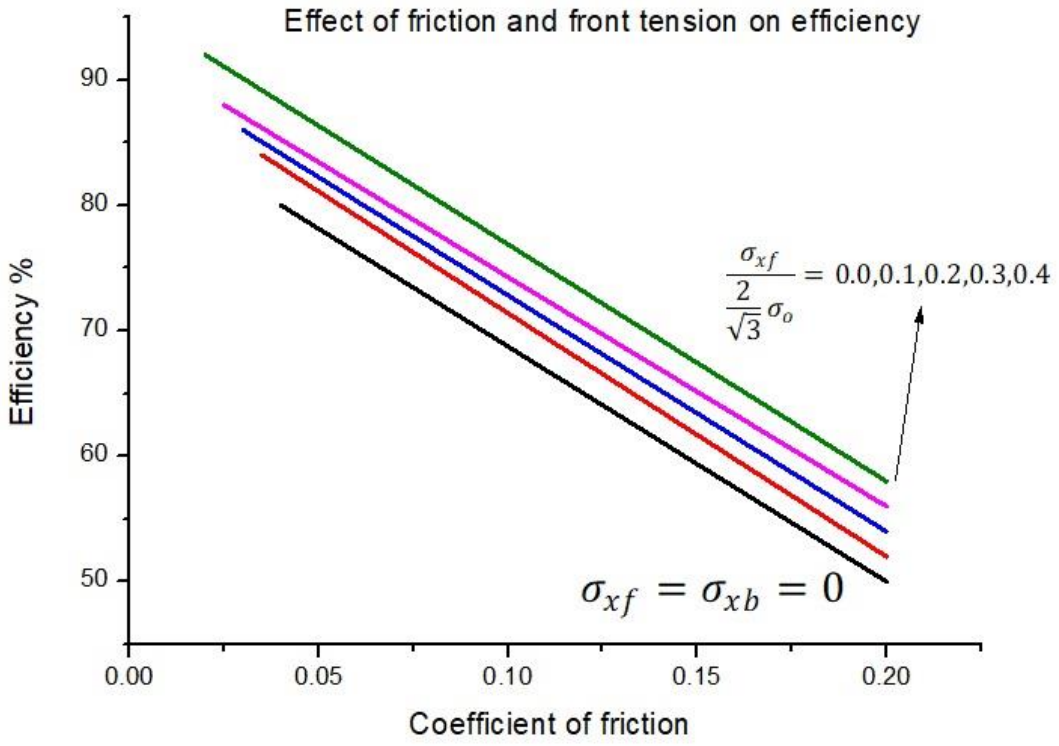

Fig. 11. Effect of friction and front tension on efficiency

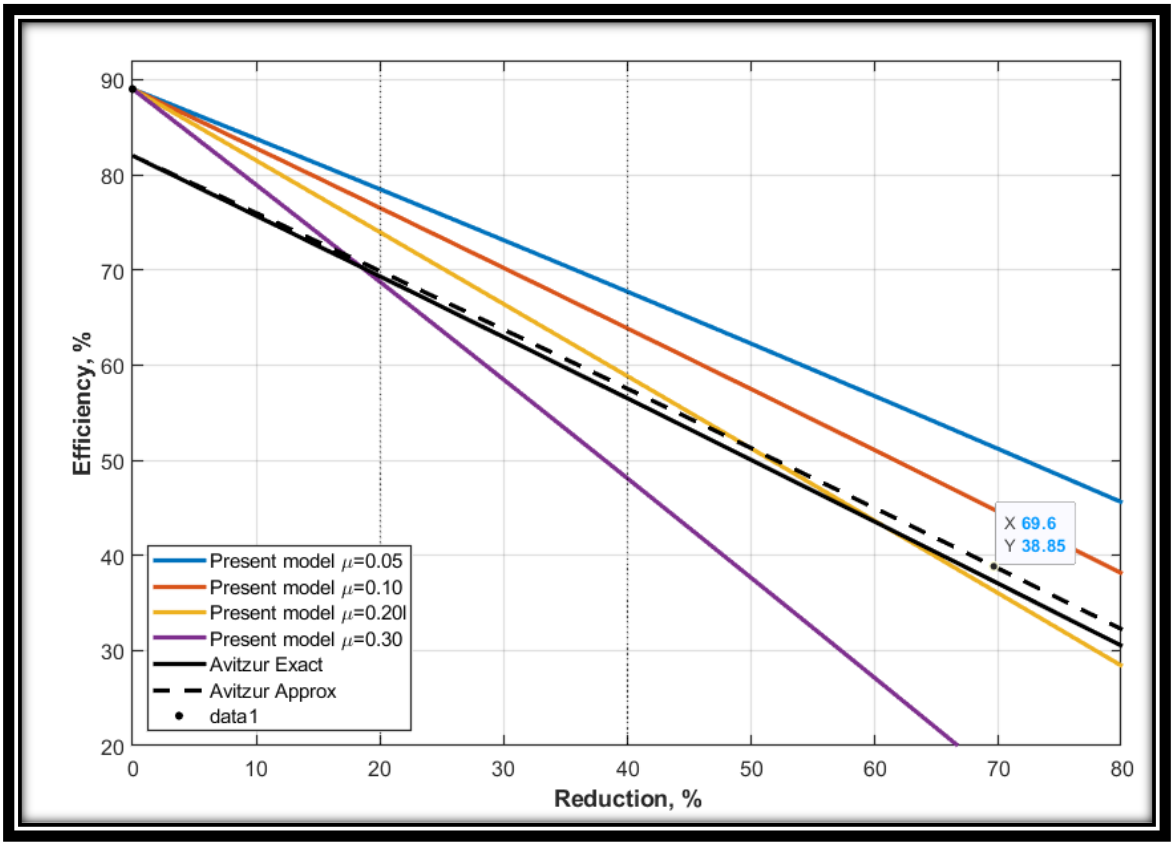

Fig. 12. Comparison of reduction vs efficiency values with Avitzur and present model

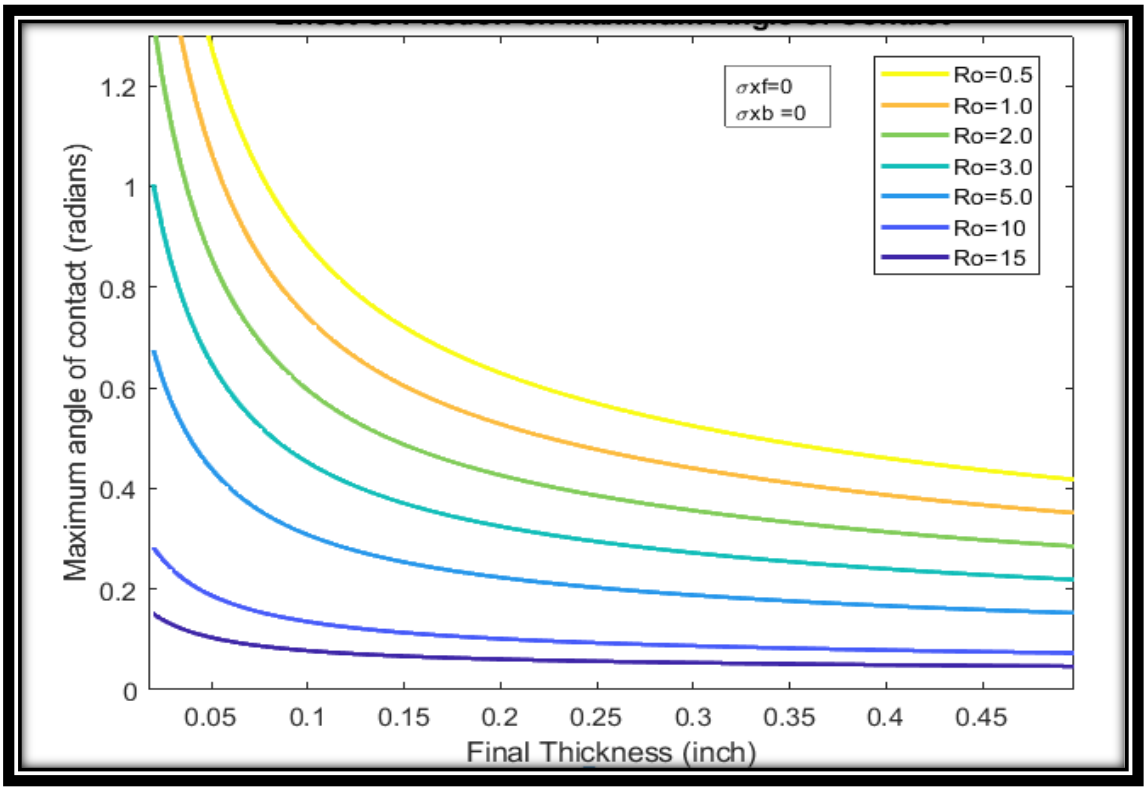

Fig. 13. Maximum length vs final thickness with Avitzur and present model

3. Conclusions

- Using a modified slab approach, a thorough analytical framework for asymmetric cold strip rolling has been created that can capture intricate deformation characteristics resulting from roll speed mismatch, frictional asymmetry, and applied tensions. Compared to traditional symmetric or partially asymmetric formulations, the suggested model provides a more physically representative description of material flow by methodically identifying three distinct deformation regions: forward slip zone, cross shear zone, and backward slip zone.
- For both upper and lower rolls, closed-form solutions for rolling pressure, rolling force, and rolling torque are made possible by the derived equilibrium equations and boundary conditions. According to parametric analysis, deformation behavior, neutral point locations, and load requirements are strongly and coupledly influenced by roll speed ratio, frictional stress distribution, and front-back tension combinations. When forward friction predominates over backward friction, an increase in roll speed ratio consistently lowers rolling force and torque, indicating favorable energy transfer conditions and improved process efficiency.
- The current formulation predicts smoother pressure distributions and more realistic torque trends, particularly under high asymmetry conditions, according to a comparative evaluation with well-established analytical models. A major drawback of previous slab-based models is addressed by the inclusion of cross shear effects, which greatly increases the precision of stress and power estimates.
- The roll speed ratio, which has an ideal value of about 80%, is the most important control parameter influencing rolling performance, according to grey relational analysis. Front tension's contribution comes in second. By minimizing rolling force and torque, the optimized parameter set lowers energy consumption, improves strip surface quality, and lessens roll surface damage.
- The robustness of the proposed model is reinforced by validation through confirmation tests, which show close agreement between analytical predictions and optimized outcomes. With direct relevance to industrial applications involving high-strength alloys and sophisticated rolling configurations, the developed

analytical approach offers a dependable and computationally efficient tool for the design, optimization, and control of asymmetric cold rolling processes.

Conflict of Interest

The authors declare that there is no conflict of interest regarding the publication of this paper. The funding agency had no role in the design of the study; collection, analysis, or interpretation of data; writing of the manuscript; or decision to publish the results.

Acknowledgments

The authors Gopalakrishnaiah, gratefully acknowledge the PVP Sidhartha, Vijayawada and Andhra University to the fabrication, analysis and further performance studies. The authors thank to Srinivasarao for providing analytical knowledge for mathematical models. Gopalakrishnaiah mentioned thanks to Principal, Dept. of ME, PVP Sidhartha, Vijayawada, India for utilizing initial monitoring of rolling set-up and other financial facilities.

References

[1] B. Avitzur, "Power analysis of cold strip rolling," *J. Manuf. Sci. Eng. Trans. ASME*, vol. 85, no. 1, pp. 77–88, 1963, doi: 10.1115/1.3667599.
[2] B. Avitzur, "An upper-bound approach to cold-strip rolling," *J. Manuf. Sci. Eng. Trans. ASME*, vol. 86, no. 1, pp. 31–45, 1964, doi: 10.1115/1.3670446.
[3] Z. C. Lin and V. H. Lin, "Analysis of the variation of the cold-rolling characteristics of rolling force, strip shape, stress and temperature, for a three-dimensional strip," *J. Mater. Process. Tech.*, vol. 54, no. 1–4, pp. 326–340, 1995, doi: 10.1016/0924-0136(95)01796-8.
[4] J. W. Baxter and J. R. Bumby, "Proceedings of the Institution of Mechanical Engineers, Part I: Journal of Systems and Control Engineering," 1995, doi: 10.1243/PIME.
[5] F. A. R. Al-Salehi, T. C. Firbank, and P. R. Lancaster, "An experimental determination of the roll pressure distributions in cold rolling," *Int. J. Mech. Sci.*, vol. 15, no. 9, pp. 693–710, 1973, doi: 10.1016/0020-7403(73)90049-0.
[6] H. Altinkaya *et al.*, "Power analysis of cold strip rolling," *Int. J. Mech. Sci.*, vol. 38, no. 1, pp. 19–32, 1996, doi: 10.1016/S0020-7403(01)00086-8.
[7] B. Avitzur and W. Pachla, "The upper bound approach to plane strain problems using linear and rotational velocity fields—part I: Applications," *J. Manuf. Sci. Eng. Trans. ASME*, vol. 108, no. 4, pp. 307–316, 1986, doi: 10.1115/1.3187081.
[8] E. R. Lambert, H. S. Mehta, and S. Kobayashi, "A new upper-bound method for analysis of some steady-state plastic deformation processes," *J. Manuf. Sci. Eng. Trans. ASME*, vol. 91, no. 3, pp. 731–740, 1969, doi: 10.1115/1.3591677.
[9] N. H. Barbosa-Filho, "A note on the theory of demand-led growth," *Contrib. Polit. Econ.*, vol. 19, no. 1, pp. 19–32, 2000, doi: 10.1093/cpe/19.1.19.
[10] S. H. Hsiang and S. L. Lin, "Study of a 3-D FEM combined with the slab method for shape rolling," *J. Mater. Process. Technol.*, vol. 100, no. 1, pp. 74–79, 2000, doi: 10.1016/S0924-0136(99)00369-6.
[11] "a slab method software for the numerical simulation of mixed lubriction regime in cold strip rolling.pdf."
[12] M. Oh and N. Kim, "Optimum design of roll forming process of slide rail using design of experiments," *J. Mech. Sci. Technol.*, vol. 22, no. 8, pp. 1537–1543, 2008, doi: 10.1007/s12206-008-0430-9.
[13] Z. C. Lin *et al.*, "Calculation of rolling pressure distribution and force based on improved Karman equation for hot strip mill," *J. Manuf. Sci. Eng. Trans. ASME*, vol. 38, no. 1, pp. 293–305, 2014, doi: 10.1016/j.ijmecsci.2014.09.011.
[14] H. Haghighat and P. Saadati, "An upper bound analysis of rolling process of non-bonded sandwich sheets," *Trans. Nonferrous Met. Soc. China (English Ed.*, vol. 25, no. 5, pp. 1605–1613, 2015, doi: 10.1016/S1003-6326(15)63764-5.
[15] S. I. Oh and S. Kobayashi, "An approximate method for a three-dimensional analysis of rolling," *Int. J. Mech. Sci.*, vol. 17, no. 4, pp. 293–305, 1975, doi: 10.1016/0020-7403(75)90010-7.
[16] K. F. Kennedy, "An approximate three-dimensional metalflow analysis for shape rolling," *J. Manuf. Sci. Eng. Trans. ASME*, vol. 110, no. 3, pp. 223–231, 1988, doi: 10.1115/1.3187873.

[17] J. Paralikas, K. Salonitis, and G. Chryssolouris, "Optimization of roll forming process parameters-A semi-empirical approach," *Int. J. Adv. Manuf. Technol.*, vol. 47, no. 9–12, pp. 1041–1052, 2010, doi: 10.1007/s00170-009-2252-z.
[18] Z. Y. Jiang and A. K. Tieu, "A simulation of three-dimensional metal rolling processes by rigid-plastic finite element method," *J. Mater. Process. Technol.*, vol. 112, no. 1, pp. 144–151, 2001, doi: 10.1016/S0924-0136(01)00572-6.
[19] I. J. Freshwater, "Simplified theories of flat rolling - I. The calculation of roll pressure, roll force and roll torque," *Int. J. Mech. Sci.*, vol. 38, no. 6, pp. 633–648, 1996, doi: 10.1016/s0020-7403(96)80006-3.
[20] I. J. Freshwater, "Simplified theories of flat rolling - II. Comparison of calculated and experimental results," *Int. J. Mech. Sci.*, vol. 38, no. 6, pp. 649–660, 1996, doi: 10.1016/s0020-7403(96)80007-5.
[21] Orowan, E., "The calculation of roll pressure in hot and cold flat rolling," *Proc. Inst. Mech. Eng.*, vol. 150, pp. 140–167, 1943.
[22] Sims, R. B., "The calculation of roll force and torque in hot rolling mills," *Proc. Inst. Mech. Eng.*, vol. 168, pp. 191–200, 1954.
[23] Bland, D. R., and Ford, H., "The theory of rolling with front and back tension," *Proc. Inst. Mech. Eng.*, vol. 159, pp. 144–153, 1948.
[24] Hill, R., *The Mathematical Theory of Plasticity*, Oxford University Press, Oxford, 1950.
[25] Avitzur, B., *Metal Forming: Processes and Analysis*, McGraw-Hill, New York, 1968.
[26] Stone, M. D., and Gray, J. B., "Analysis of power requirements in cold rolling," *J. Eng. Ind.*, Trans. ASME, vol. 90, no. 3, pp. 521–528, 1968.
[27] Tselikov, A. I., and Smirnov, V. V., *Rolling of Metals*, MIR Publishers, Moscow, 1967.
[28] Roberts, W. L., *Cold Rolling of Steel*, Marcel Dekker, New York, 1978.
[29] Alexander, J. M., and Brewer, R. C., *Manufacturing Properties of Materials*, Van Nostrand, London, 1963.
[30] Zienkiewicz, O. C., and Godbole, P. N., "Flow of plastic materials between rough plates," *J. Mech. Phys. Solids*, vol. 18, no. 2, pp. 121–138, 1970.
[31] Li, C. S., and Kobayashi, S., "Rigid-plastic finite element analysis of plane strain rolling," *J. Eng. Ind.*, Trans. ASME, vol. 104, no. 1, pp. 55–63, 1982.
[32] Dewhurst, P., and Collins, I. F., "A matrix method for analysis of rolling processes," *Int. J. Mech. Sci.*, vol. 17, no. 4, pp. 243–255, 1975.
[33] Hill, R., "On the mechanics of rolling thin strip," *Q. J. Mech. Appl. Math.*, vol. 7, no. 1, pp. 19–31, 1954.
[34] Misaka, Y., and Yoshimoto, T., "Formulation of mean resistance to deformation of steel," *J. Jpn. Soc. Technol. Plast.*, vol. 8, pp. 414–422, 1967.
[35] Wusatowski, Z., *Fundamentals of Rolling*, Pergamon Press, Oxford, 1969.
[36] Kobayashi, S., Oh, S. I., and Altan, T., *Metal Forming and the Finite-Element Method*, Oxford University Press, New York, 1989.